Visible thermal emission from sub-band-gap laser excited cerium dioxide particles

Richard D. Robinson, Jonathan E. Spanier,[a] Feng Zhang, Siu-Wai Chan, and Irving P. Herman[b]
Materials Research Science and Engineering Center and the Department of Applied Physics and Applied Mathematics, Columbia University, New York, New York 10027

(Received 14 January 2002; accepted for publication 23 May 2002)

Cerium dioxide particles excited in air with sub-band-gap radiation emit very broad radiation in the visible spectrum above a threshold intensity that decreases with increasing ambient temperature. Concomitant with this emission is the near disappearance of the Stokes and anti-Stokes Raman scattering peaks. Both phenomena are reversible in air up to just above threshold, and are seen for nanoparticles and several-micron-diameter particles with particle diameter comparable to or smaller than the laser focus. Temperature estimates using the Stokes/anti-Stokes scattering intensity ratio suggest there is laser heating due to small intragap absorption and possible nonlinear processes, given the very slow thermal conduction. The broad emission in this loose powder may well be due to thermal emission, on the basis of spectral fitting of the high-energy part of the spectrum to a blackbody radiator at ~1200–1400 °C, although luminescence from a new phase is a possibility. The sudden decrease in Raman scattering and increase in emission in air are consistent with a transition to a new, possibly luminescent, phase, as is the continued disappearance of the Raman peaks in forming gas when the laser power is reduced below the upstroke threshold. Oxygen point defects and their complexes may play an important role in many of these processes. © *2002 American Institute of Physics.* [DOI: 10.1063/1.1494130]

I. INTRODUCTION

The optical properties of small particles have become increasingly important with the realization that linear and nonlinear optical properties of nanoparticles can be tuned by varying the quantum confinement of carriers[1] and the recent demonstrations of electrical and optical pumping of lasers with powders as the lasing media.[2,3] Cerium oxide particles are of interest because of possible applications in catalysis[4] and fuel cell technologies.[5] Oxygen defects in these particles make them complex to understand, yet useful. During an examination of strain, phonon confinement, and phonon decay in cerium dioxide nanoparticles using Raman scattering with laser radiation below the band gap,[6] the authors first observed (but did not report) unexpected broadband visible emission at higher laser power accompanied by near disappearance of the Raman peaks. In this paper we attribute this very unusual optical emission to heating and thermal emission.

II. EXPERIMENTAL METHODS

Cerium dioxide particles were synthesized by using the room temperature reaction of cerium nitrate and hexamethylenetetramine, as detailed in Ref. 7. These loose powders are placed on a glass slide and irradiated by several mW of cw ion laser radiation focused to a spot radius of ~2 μm. Most experiments were conducted with radiation at 488 nm from a cw argon ion laser; irradiation with the 514.5 nm argon ion laser line and the 337.5–356.4 nm UV lines (called ~350 nm) from a cw krypton ion laser was also briefly studied. Unpolarized Raman scattering and emission were collected in backscattering configuration and analyzed by a 0.1 m monochrometer (Ocean Optics USB2000) with a Si charge coupled device (CCD) array detector (usual acquisition time is ~1 s). Emission was also analyzed as a function of substrate temperature T using a heating stage (Linkham THMS 600) (−190–550 °C); survey measurements were also made up to 1150 °C with a different heating stage (Linkham TS1500). Transmission through and elastic scattering from a 20-μm-thick powder of 10-nm-diam particles on a transmission electron microscope grid (holey carbon) atop a glass slide were also monitored as a function of laser power using a power meter. Absorption of the nanoparticles in solution during synthesis was measured from 300 to 1100 nm using a Xe lamp at room temperature. X-ray diffraction (XRD) measurements were made on bulk cerium dioxide (5-μm-diam) up to 1300 °C using a Scintag X2 diffractometer equipped with a heating stage.

III. RESULTS

Broad visible emission from 6–25 nm and 5 μm diameter cerium dioxide particles is seen above a threshold power (fixed 2 μm focus) with 488 nm excitation in air (Fig. 1). With the substrate at room temperature (25 °C), the threshold power is ~20–25 mW for all of these particles. (Powers are cited because of uncertainties and spatial variations in the intensity.) There are run-to-run variations in the threshold

[a]Currently with the Department of Chemistry and Chemical Biology, Harvard University.
[b]Contact by e-mail at iph1@columbia.edu

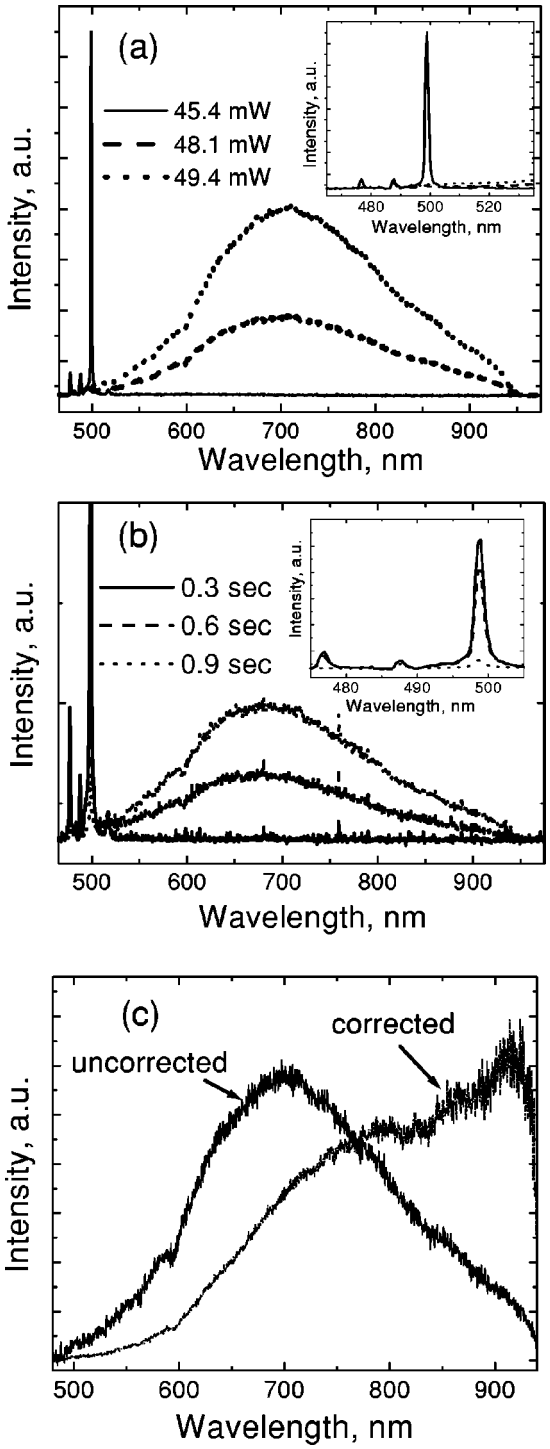

FIG. 1. Emission (a,b,c) and Raman scattering (a,b) from 5 μm cerium dioxide particles excited using 488 nm in air. The insets to (a,b) show the Stokes peak (499 nm), elastically scattered light (488 nm), and the anti-Stokes peak (477 nm); (a) below and above threshold powers for a -190 °C substrate temperature; (b) emission spectra are integrated for 0.3 s up to 0.3, 0.6, and 0.9 s using 26 mW with a room temperature substrate; (c) emission spectra using 36 mW with a room temperature substrate, uncorrected and corrected for grating and CCD array spectral responses. The emission spectra in (a,b) are uncorrected.

power, but all trends reported here and below are consistent within a series of runs. Above this threshold power (at 488 nm), the first-order Raman signal at the triply-degenerate 464 cm^{-1} mode decreases by a factor of 10–100 (Fig. 1(a), 1(b)

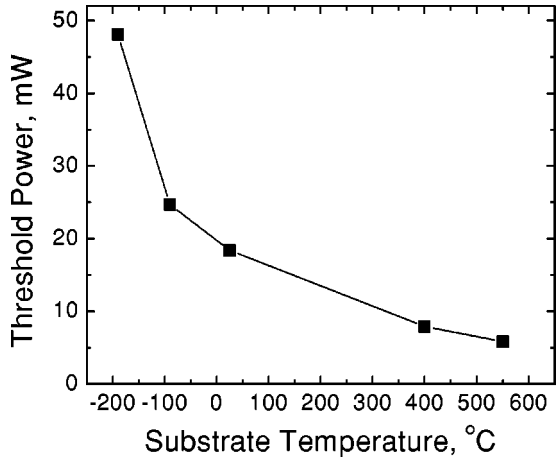

FIG. 2. Threshold power vs substrate temperature for 5 μm particles in air (488 nm).

insets). These correlated changes occur with the substrate temperature varied from -190 to 550 °C. Figure 1(c) shows the broad emission peaks near 700 nm and is ~300 nm wide full width at half maximum, without correction for the grating and CCD detector spectral responses. After spectral calibration, the emission is seen to peak at longer wavelengths >900 nm, and likely deeper in the infrared. Above threshold the spectral shape of the emission profile is roughly the same, independent of substrate temperature, but the emission intensity increases with power. No broadband emission is seen from pellets prepared from sintering these 5 μm powders. Emission is seen with a much higher threshold from pellets made from the nanoparticles.

When the laser power is near threshold, emission occurs in ~1 min; with power much higher than threshold it occurs within <1 s [Fig. 1(b)]. When the laser power is decreased below threshold, the emission disappears within the 1 s observation time scale. For variable incident power approaching and just above threshold, there is reversibility in the Raman intensity, peak position, and linewidth in air without hysteresis. The threshold for broadband emission using 488 nm excitation of the particles in air decreases with increasing substrate temperature from ~48 mW at -190 °C to 6 mW at 550 °C (Fig. 2). Examination at higher substrate temperatures (to 1150 °C), shows a narrow power range below emission threshold within which Raman scattering intensities are decreased greatly with no broadband emission. Large background thermal emission prevented detailed Raman analysis at these higher substrate temperatures. All these above experiments were performed in air ambient.

When argon is flowed through the cell, eliminating most of the oxygen, water vapor, nitrogen, etc., the emission occurs with the same spectral profile and the effective loss of the Raman signal. When forming gas (95% N_2, 5% H_2) is flowed through the cell, with the substrate at room temperature, the Raman signal disappears and emission appears above a threshold; the Raman signal then reappears when the power is lowered below this upstroke threshold, as with air and argon. However, with the substrate at 550 °C, when the laser power is lowered below the upstroke threshold (~8 mW), say to ~2 mW, the emission disappears and, for form-

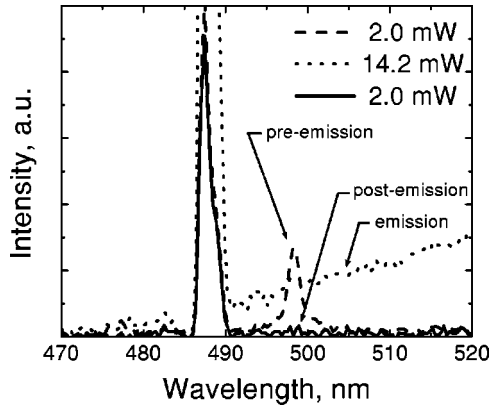

FIG. 3. Stokes Raman peak at 499 nm with irradiation of 5 μm particles in forming gas with the substrate at 550 °C (488 nm). Spectra are shown for a time sequence, with the laser first below threshold (2.0 mW, pre-emission), then above threshold (14.2 mW, emission), and later below the upstroke threshold (2.0 mW, post-emission).

ing gas only, the Raman signal is still absent (Fig. 3). Just above threshold, the (uncorrected) emission peaks near 800 nm in forming gas, which is to the red of that in air and argon ($\sim$700 nm), but the emission profiles are more similar much above threshold. When a water drop is added to the dry powder, in an air ambient at room temperature, the threshold power doubles and the delay in seeing emission is longer ($\sim$1 min) than the otherwise typical $<$1 s.

Concomitant with the appearance of visible emission is the near disappearance of the normally strong 464 cm^{-1} Raman peaks in every case. The inset to Fig. 1(a) shows the Stokes (S) (499 nm) and anti-Stokes (AS) (477 nm) Raman peaks below and above threshold in air, along with the same elastic scatter in all regimes; in Fig. 1(b) the increase in emission in time ($<$1 s) is accompanied by a decrease in S and AS Raman peaks, but no significant change in elastic scatter. The ratio of the peak intensities of these S and AS peaks is monitored as a function of power for various substrate temperature in Fig. 4(a). These intensities are corrected for spectral sensitivity and the limited number of pixels in each profile (discreteness); additional corrections are discussed later. There is a power range above threshold for which this process is reversible in air, with the reappearance of the Raman signals when the laser power is decreased below threshold. Above a certain limit, it is irreversible, with the Raman signal in some cases stronger or weaker than before the process began. Also, as the laser power is increased towards the threshold value, there is a reversible decrease in Raman shift.

Transmission of the focused laser through 20-μm-thick samples of unpacked powder (10-nm-diam) in air (with losses due to absorption and scattering) [Fig. 5(a)] and backward elastically scattered light [Fig. 5(b)] are also monitored as a function of laser power. Small changes in each are seen at the emission threshold as the power is increased (upstroke). In Fig. 5(b) no sudden change is seen in the downstroke, but such a change is sometimes seen in other runs. No changes are seen in the upstroke with an unfocused beam.

At room temperature, similar broadband visible emission from the particles in air is also seen using 514.5 nm and with

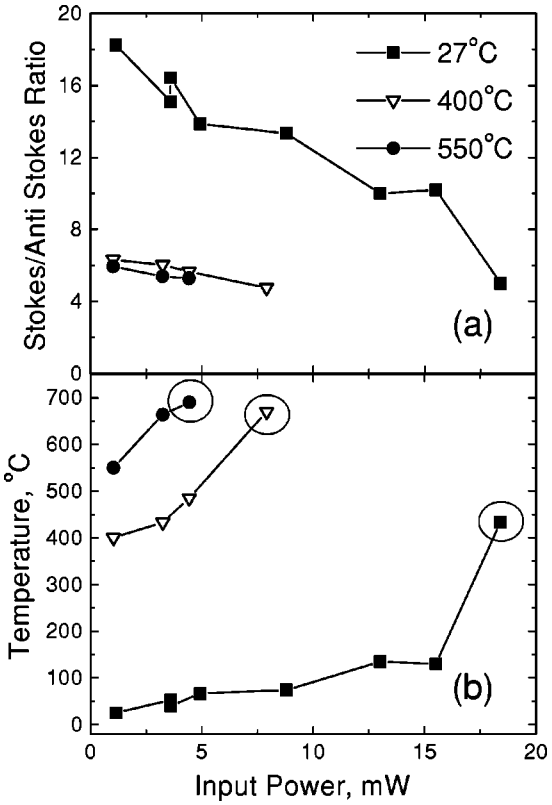

FIG. 4. (a) Stokes/anti-Stokes intensity ratios as a function of laser power (5 μm particles, 488 nm, air), for different substrate temperature, and (b) the local averaged temperature from these ratios (the data points at the emission thresholds are circled).

$\sim$350 nm excitation (not shown), with a concomitant decrease in the Raman signal. The short wavelength onset of emission from $\sim$350 nm excitation (about 550–600 nm) is longer than for 488 nm excitation (about 500 nm), while the

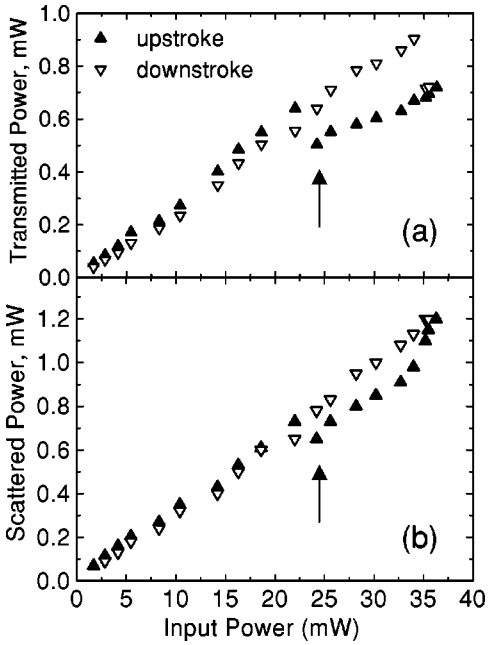

FIG. 5. (a) Transmission and (b) backward elastically scattered focused 488 nm light as a function of incident power (10-nm-diam particles in air at room temperature). The arrows show the threshold for emission.

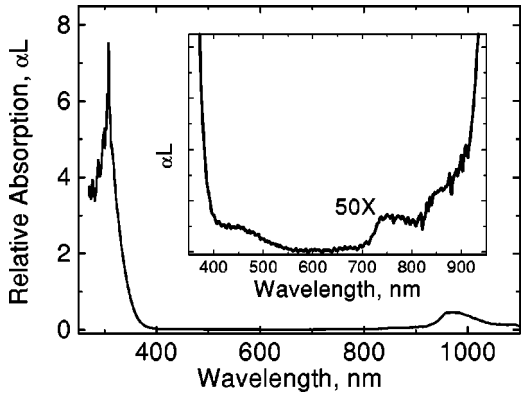

FIG. 6. Absorption of ~5-nm-diam cerium dioxide nanoparticles, showing the weak linear absorption at 488 nm in the inset.

threshold power is about the same for both with the substrate at room temperature (~25 mW). No sharper emission features usually attributable to exciton recombination, band–band emission, or near-band defects are seen at room temperature or at −190 °C for any of the excitation wavelengths.

The relative absorption of the nanoparticles of diameter ~5 nm collected after a 1 hour synthesis is shown in Fig. 6. (The effect of absorption of the solvent has been removed.) The spectrum shows strong band edge absorption near 350 nm and weak absorption peaked near 750 nm (inset, expanded vertical scale) which is ~200 times weaker than the peak band edge absorption near 300 nm. This figure and the absorption spectra of Ref. 7 during particle growth show that irradiation at 488 and 514.5 nm is sub-band-gap, while that ~350 nm excitation is near the band edge (depending on particle size). [In Ref. 7, the absorption band in ~6-nm-diam particles began at ~360 nm (3.4 eV) and peaked at ~335 nm (3.7 eV), representing blue shifts from the 393 nm (3.15 eV) band attributed to absorption from the valence band of O_{2p} character to the Ce_{4f} narrow band.][8]

No evidence of a phase change is supported by the x-ray diffraction of bulk cerium dioxide up to the maximum temperature studied (1300 °C) in room ambient.

IV. DISCUSSION

A. Particle heating

Most of these observations point to the importance of laser absorption and heating of the particles as the source of the emission. (1) Emission is seen for particles smaller or comparable to the several μm focus of the laser, but not for the pellets made from 5 μm particles. (2) When a water droplet is placed on top of the pile, the threshold power increases. (The water increases thermal conduction, but also affects laser focusing and particle density.) (3) The emission threshold decreases as the substrate temperature is increased. (4) A particle temperature rise is seen with increasing laser power, as determined from the S/AS intensity ratio (see below). (5) The Raman shift decreases with increasing laser power up to threshold, which suggests an increase in temperature.[6] The first two observations are consistent with a large temperature rise in the particles even with weak absorption, because of the importance of the small thermal conductivity of air for the unpacked particles. There is greater thermal conductivity with water present or within the large particle pellets (with only a small laser heated region). One exception to the first point is that emission is seen for a pellet made from nanoparticles, although at much higher threshold power.

The S/AS intensity ratio of Raman scattering at 464 cm^{-1} in Fig. 4(a) is used to semiquantitatively determine the temperature of the irradiated region (488 nm). This ratio is $A\exp(E/kT)$,[9] where E is the phonon energy and A is a parameter currently taken to be unity. The estimated temperature rise is shown in Fig. 4(b) assuming a uniform T profile, as a function of incident power for the three substrate temperatures; the circled data points denote the first measured power at which photoluminescence (PL) appears for each substrate temperature. Below threshold this ratio decreases with increasing laser intensity, suggesting T in the irradiated region increases roughly linearly with power at low power and faster than linearly near threshold. Analysis of the data in this manner, suggests an increase in T from 25 °C to ~440 °C just below threshold.

However, this is clearly an underestimate of the peak T since the S and AS scattered light are collected over the spatially-varying temperature profile of the heated spot. If the temperature rise linearly followed the Gaussian spatial profile of the laser intensity, the temperature rise at the center would be about twice that predicted from ratio of the total S and AS signals. This suggests the increase in T at the center is about 830 °C. Including thermal conduction, the peak T rise would be less than this if the thermal conductivity were independent of T or increased with T (as for bulk insulators), or even larger than this if thermal conductivity decreased with T (as for semiconductors). If superlinear absorption were important, the peak T rise would again be even larger relative to the averaged T obtained from the S/AS measurements.

The small changes in Raman shift with temperature, $E(T)$[6] affect the temperature estimates relatively little. There are other well-documented uncertainties in using this S/AS ratio as a monitor of temperature, which arise from the temperature dependences of the ratios of the optical parameters in A.[9] The assumption that A is unity here seems reasonable since the excitation wavelength is below the band gap and far from the band edge.

B. Origin of the emission

These observations point to the importance of laser heating, but not to the source of the emission. Figure 7 shows the short-wavelength part of the emission <700 nm (which is relatively insensitive to the spectral calibration correction) matches blackbody emission with $T \sim 1200-1400$ °C (with no emissivity corrections) for 488 nm excitation in air, which would peak at ~2 μm; this T is much less than the 2450 °C melting point for bulk cerium dioxide. These temperature estimates are consistent with the S/AS measurements, given their uncertainties. Emission curves with three excitation powers above threshold and the blackbody curves are each normalized to unity at 700 nm. In forming gas, the short-

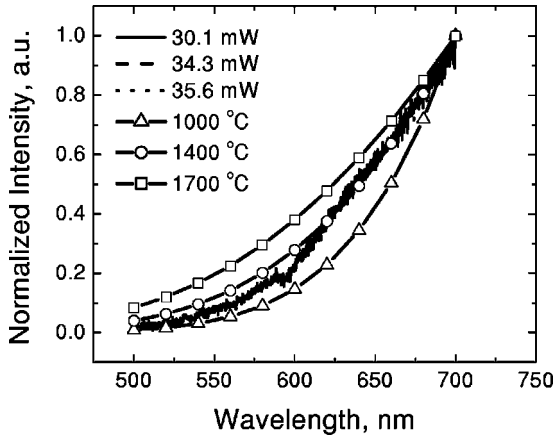

FIG. 7. Comparison of short-wavelength edge of emission at various powers (5 μm particles in air, 488 nm) and thermal emission spectra (emissivity $=1$), each normalized to unity at 700 nm.

wavelength part of the emission matches a blackbody radiator at a lower temperature, ~1000 °C. Thermal emission has been observed many times in above-band-gap laser-excited particles. This is commonly known as laser-induced incandescence, and has been used in many studies of soot and a study of metal nanoparticles to determine particle concentration, sizes, and temperature.[10,11] The small dip in the emission curves at 595 nm in Figs. 1 and 7 is apparently not instrumental in nature and is unexplained. At these temperatures, thermal radiation losses are estimated to be orders of magnitude smaller than thermal conduction losses.

It is possible that this emission is not thermal radiation, but luminescence from a high-temperature phase of CeO_y. This would explain why the shape of the emission profile does not change much with laser power. However, the different short-wavelength limits of the emission in air for the three different excitation wavelengths suggest this is not the correct scenario. The experiments in forming gas with elevated substrate temperature suggest a new reduced phase could be created since the Raman signal remains absent during a laser power downstroke below the upstroke threshold. Since the visible emission then disappears, this suggests that the emission is not due to luminescence that is linear with the laser power. It is likely, but not definite, that the same phase is created at higher laser powers in air, argon, and forming gas. Also, one would expect different thresholds to a new phase for different particle sizes. Emission could also arise from defect states in the band gap; this could cause a nonlinear dependence of emission intensity on laser intensity related to the saturation of these states. However, this is inconsistent with the short-wavelength emission limit being shorter for 488 nm excitation in air than with ~350 nm excitation. Finally, the emission spectral widths are very large, and are much larger than expected from most band or defect emissions even at high *T*.

C. Decrease in Raman signals

Above threshold the Raman peak intensities decrease by a factor of 10–100. The Raman scattered intensity from a semi-infinite medium is approximately proportional to $(1-R_1)(1-R_2)|\chi|^2/(\alpha_1+\alpha_2)$,[9] where R is the reflection coefficient, χ is the Raman susceptibility, α is the attenuation coefficient (including loss due to absorption and elastic scattering), 1 refers to the input light, and 2 to the scattered light wavelengths. Therefore, the Raman signals can decrease at threshold power because there is: (1) more reflection, (2) more absorption, so there is less penetration of light into (or out of) the sample, and/or (3) a decrease in the Raman susceptibility. All of these usually change gradually with temperature.

A very large change in the last two factors could be due to a change in the type of material: new composition or a change in phase. Since the Raman profile is already broad for the nanoparticles (but not the larger particles)—due to confinement and strain — and already samples much of the Brillouin zone, a change to an amorphous material would decrease the peak intensity of the Raman peak for nanoparticles relatively little. After a structural phase change the Raman peak energy of the mode can shift or the mode may become weaker or forbidden. This could account for a sudden increase in heating with power leading to thermal emission or to a luminescing phase. However, XRD up to 1300 °C suggests no phase changes in bulk cerium dioxide. This measurement is sensitive to the relative positions of the Ce atoms; structural transitions involving the oxygen atoms cannot be ruled out. However, the continued absence of the Raman peaks when cerium dioxide is heated in forming gas (heated substrate) and the laser power is decreased below the upstroke threshold power suggests that a reduced CeO_y ($y<2$) phase is formed at higher power.

A sudden change in temperature with power due to nonlinear absorption in a given phase could also account for some of these changes, but the S/AS intensities ratios suggest a relatively gradual change with power to threshold. The transmission and scattering data in Fig. 5 suggest only a small increase in reflection, elastic scattering and/or absorption at threshold, too small to account for the change of Raman scattering (first two causes). No other Raman peaks appear above threshold. The weak residual Raman scattering above threshold is likely scattering from the wings of the focused laser.

The S/AS measurements suggest that the absorption is linear at lower powers and possibly superlinear (as with two-photon or thermal-induced absorption) at higher powers. Figure 6 shows there is weak linear sub-band-gap absorption, which seems too weak to lead to this large heating.

D. Other points

In an unpublished study,[12] Weber observed an abrupt loss of the 464 cm^{-1} Raman line and the appearance of visible emission in cerium dioxide particles under reducing conditions around 600 °C. This was done with a weakly focused 632.8 nm He-Ne line, so laser heating was likely insignificant. These observations are fairly consistent with those here in that they suggest a phase transition at elevated temperature; they also suggest luminescence from that new phase.

Many of the useful properties of cerium dioxide particles originate from the oxygen vacancies. For example, an ability

to form and annihilate oxygen vacancies can help control CO oxidation to CO_2, and NO_x reduction to N_2. The fractional population of these defects increases with smaller particle size,[7] which is very significant for applications of nanoparticles. Since the observations here for nm- and μm-sized particles were very similar, it would not seem that defects play a big role unless they are generated by the laser irradiation. Laser irradiation may generate further substantial powder heating by the generation of point defects and electronic carriers. This effect is assisted with higher sample temperatures. The buildup time [Fig. 1(b)] could suggest a buildup of defects. If these defects were important, it could help explain a possible phase transition at elevated temperatures. The phase diagram for bulk CeO_y with $y=2$ shows no transitions to $>1400\,°C$ and transitions from 400–700 °C for $1.82<y<2.0$.[13,14]

It is possible that the laser irradiation induces Frankel defect pairs, i.e., oxygen interstitial and vacancy pairs of CeO_2. These defect pairs and complexes are usually not observed in bulk ceramics until high *T*, but they have been observed in La_2O_3-doped CeO_2 nanoparticles by neutron scattering.[15] (Loss of oxygen has been observed during high-temperature sintering of cerium dioxide particles, reducing CeO_2 to Ce_2O_3.)[16] At the same time it is possible that electron–hole pairs are also generated through sub-band-gap laser irradiation because of mid-band-gap states from local point defects at high *T*. These electronic carriers give extra electrostatic screening to these point defects and lower both the formation and migration energies. With much lower migration energies, these defects are more prompt to ordering and forming associated defect complexes. Ordering of oxygen vacancies along one of the four $\langle 111\rangle$ directions can reduce the original cubic symmetry to rhombohedral R3 (the Ce_7O_{12} phase) locally or to any one of the Ce_nO_{2n-2} phases locally. The resulting different modes and Raman susceptibilities may explain the disappearance of the Raman peaks and their reappearance after irradiation.

Note the high temperature stability of cerium dioxide in air once made it the emission component of an illumination source[17] that was seriously considered for commercialization over a century ago. Thermal emission from cerium and thorium oxide mantles heated by flames was evaluated for widespread use but ultimately rejected in favor of the incandescent bulb, which had been invented just a few year earlier. These mantles are currently used in lanterns for camping.

V. CONCLUSIONS

Cerium dioxide particles excited with sub-band-gap focused cw lasers emit very broad radiation in the visible above a threshold intensity that decreases with ambient temperature. Concomitant with this emission in these loose powders is the near disappearance of the Stokes and anti-Stokes Raman scattering peaks. These phenomena are reversible in air just above threshold, and are caused by laser heating due to small intragap absorption and possible nonlinear processes. The broad emission may well be due to thermal emission, on the basis of spectral fitting of the high-energy part of the spectrum in air to a blackbody radiator at ~1200–1400 °C. The sudden decrease in Raman scattering with laser power suggests a possible phase transition, especially given the continued disappearance of the Raman peaks in forming gas when laser power is decreased below the upstroke threshold; luminescence from such a phase remains a possibility. Oxygen point defects and their complexes are often important in cerium dioxide and they may play a role in these observations. Future work includes studying the oxygen defect ordering with neutron scattering, since Ce ions are the only dominating scattering centers in x-ray diffraction used here.

ACKNOWLEDGMENTS

This work was supported primarily by the MRSEC Program of the National Science Foundation under Award Number DMR-9809687. The authors would like to thank D. Welch for stimulating discussions, J. Im for loaning the high-temperature heating stage, and B. (W. H.) Weber for discussions about his unpublished results (Ref. 12). One of the authors (R. D. R.) thanks the Ford Foundation for its support.

[1] See for example, C. B. Murray, C. R. Kagan, and C. G. Bawendi, Annu. Rev. Mater. Sci. **30**, 545 (2000).
[2] H. Cao, J. Y. Xu, E. W. Seelig, and R. P. H. Chang, Appl. Phys. Lett. **76**, 2997 (2000).
[3] G. R. Williams, S. B. Bayram, S. C. Rand, T. Hinklin, and R. M. Laine, Phys. Rev. A **65**, 013 807 (2002).
[4] A. Tschope, W. Liu, M. Flytzani-Stephanopolous, and J. Y. Ying, J. Catal. **157**, 42 (1995); M. Flytzani-Stephanopoulous, T. L. Zhu, and Y. Li, Catal. Today **62**, 145 (2000).
[5] S. Park, J. M. Vohs, and R. J. Gorte, Nature (London) **404**, 265 (2000); B. C. H. Steele, Solid State Ionics **12**, 391 (1984).
[6] J. E. Spanier, R. D. Robinson, F. Zhang, S.-W. Chan, and I. P. Herman, Phys. Rev. B **64**, 245 407 (2001).
[7] F. Zhang, S.-W. Chan, J. E. Spanier, E. Apak, Q. Jin, R. D. Robinson, and I. P. Herman, Appl. Phys. Lett. **80**, 127 (2002).
[8] L. Fangxin, W. Chengyun, S. Qingde, Z. Tianpeng, and Z. Guiwen, Appl. Opt. **36**, 2796 (1997).
[9] G. E. Jellison, D. H. Lowndes, and R. F. Wood, Phys. Rev. B **28**, 3272 (1983).
[10] A. C. Eckbreth, J. Appl. Phys. **48**, 4473 (1977).
[11] R. L. Vander Wal, T. M. Ticich, and J. R. West, Appl. Opt. **38**, 5867 (1999).
[12] W. H. Weber, private communication.
[13] G. Adachi and N. Imanaka, Chem. Rev. **98**, 1479 (1998).
[14] E. A. Kummerle, F. Guthoff, W. Schweika, and G. Heger, J. Solid State Chem. **153**, 218 (2000).
[15] E. Mamontov and T. Egami, J. Phys. Chem. Solids **61**, 1345 (2000).
[16] Y. Zhou and M. N. Rahaman, Acta Mater. **45**, 3635 (1997).
[17] C. A. Von Welsbach, Incandescent Device, U.S. Patent No. 399,174 (5 March 1889).